Submitted to JGR - Atmospheres Aug 2000

Northern Hemisphere winter climate response to greenhouse gas, ozone, solar and volcanic forcing

Drew T. Shindell
NASA Goddard Institute for Space Studies, New York

Gavin A. Schmidt
NASA Goddard Institute for Space Studies and Center for Climate Systems Research, Columbia University, New York

Ron L. Miller
NASA Goddard Institute for Space Studies, New York

David Rind
NASA Goddard Institute for Space Studies, New York

Abstract

The Goddard Institute for Space Studies (GISS) climate/middle atmosphere model has been used to study the impacts of increasing greenhouse gases, polar ozone depletion, volcanic eruptions, and solar cycle variability. We focus on the projection of the induced responses onto Northern Hemisphere winter surface climate. Changes in the model's surface climate take place largely through enhancement of existing variability patterns, with greenhouse gases, polar ozone depletion and volcanic eruptions primarily affecting the Arctic Oscillation (AO) pattern. Perturbations descend from the stratosphere to the surface in the model by altering the propagation of planetary waves coming up from the surface, in accord with observational evidence. Models lacking realistic stratospheric dynamics fail to capture these wave flux changes. The results support the conclusion that the stratosphere plays a crucial role in recent AO trends. We show that in our climate model, while ozone depletion has a significant effect, greenhouse gas forcing is the only one capable of causing the large, sustained increase in the AO observed over recent decades. This suggests that the AO trend, and a concurrent strengthening of the stratospheric vortex over the Arctic, are very likely anthropogenic in origin

1. Introduction

Recent observations show very large increases in surface temperatures over the Northern Hemisphere continents during winter (Figure 1A). These result largely from an increase in the westerly air flow around the Northern Hemisphere, which brings warmer, wetter oceanic air over the continents. This westerly flow, and therefore the surface temperature changes, are associated with the leading variability pattern of Northern Hemisphere cold-season sea-level pressure (SLP), called the 'Arctic Oscillation' (AO) (Figure 1B). Observations show an apparent upward trend in the amplitude of this pattern, or equivalently, a bias towards the positive phase of the pattern, in recent decades [*Thompson and Wallace*, 1998; *Thompson et al.*, 2000]. The variability associated with this pattern extends from the surface up into the stratosphere, and in fact the variability pattern can be equivalently defined as being composed of variability at all levels from the surface through the lower stratosphere [*Baldwin and Dunkerton*, 1999]. Previously, we showed that only with the inclusion of a well-resolved stratosphere in our climate model were we able to reproduce the observed trend in the AO in response to increasing greenhouse gases [*Shindell et al.*, 1999a]. Consistent with those results, observations indicate that changes in the stratosphere typically precede the changes in the lower atmosphere [*Kodera and Koide*, 1997; *Baldwin and Dunkerton*, 1999]. As a result, the stratospheric climate model was better able to reproduce the large continental wintertime warming trends seen in the Northern Hemisphere than a similar 'tropospheric model'.

AO trends in the earlier climate model simulations were induced by the effect of increasing greenhouse gases on stratospheric temperatures. Other perturbations to the stratosphere also affect surface climate. For example, it has been shown that the circulation in the lower atmosphere can be affected by stratospheric changes such as large volcanic eruptions [*Rind et al.*, 1992; *Graf et al.*, 1993; *Kodera*, 1994] or solar forcing [*Haigh*, 1996, 1999; *Shindell et al.*, 1999b]. We now investigate in more detail the mechanism by which stratospheric perturbations affect surface changes. Greenhouse gas increases, volcanic aerosols, ozone depletion or solar forcing can all induce meridional temperature gradients in the stratosphere during wintertime. We demonstrate a positive feedback whereby zonal wind anomalies induced by these thermal gradients near the tropopause are amplified through planetary wave refraction. Deflection of upward-propagating tropospheric waves at lower and lower altitudes in effect carries the anomaly steadily down from the stratosphere, allowing stratospheric changes to affect surface climate by altering tropospheric energy flow.

Additionally, we examine the extent to which each individual stratospheric forcing excites with the natural patterns of variability. This is accomplished by projecting the induced changes onto empirical orthogonal functions (EOFs), fixed spatial patterns of variability ranked by the amount of variability accounted for by each pattern [e.g. *Kutzbach*, 1970], derived from a control run with no external forcings. Examination of the observations reveals that the recent trend in sea-level pressure has occurred primarily through enhancement of the AO (EOF 1) [*Thompson et al.*, 2000] and Figure 2, discussed further below). In order to reproduce the observations, it's therefore necessary that a model yield a trend in the amplitude of the AO pattern similar to the observations, while at the same time keeping the amplitudes of changes in the other variability patterns small. Analysis of our model simulations shows that while greenhouse gas increases, volcanic aerosols, or Arctic ozone depletion can excite primarily this leading mode, only increasing greenhouse gases can excite an AO trend comparable to the observed value

2. Experimental Setup

Simulations of the climate response to increasing greenhouse gases, Arctic ozone depletion, volcanic eruptions, and solar cycle variability have been performed (Table 1). These are the primary forcings that affect the stratosphere, which seems to play an important role in Northern Hemisphere winter climate change [*Shindell et al.*, 1999a]. Increases have been observed in the abundance of atmospheric greenhouse gases, Arctic winter/spring ozone loss, and solar irradiance over decadal and longer time scales [e.g. *Houghton et al.*, 1992]. Solar cycle variability is used here as a proxy for longer-term solar variations, which are not well known. While there is not thought to have been a long term increase in volcanic eruptions, those simulations complete the range of forcings, and therefore allow us to perform a systematic comparison of the mechanism by which perturbations to the stratosphere affect surface climate.

The primary model used here is an older version of the Goddard Institute for Space Studies (GISS) stratospheric climate model which has 8° × 10° de-

gree horizontal resolution, and 23 vertical layers extending up into the mesosphere (top at 0.002 mb, ≈85 km) [*Rind et al.*, 1988b, a]. While a newer version of the model, with finer resolution, is available, computational resources do not yet permit us to carry out simulations with that model for the large number of years used here. Note that the propagation of planetary waves is a largely quasi-geostrophic process, so it should not be greatly affected by resolution, especially for the longest waves which are resolved by even coarse resolutions. However, the amplitude of the waves may change with resolution, leading to quantitative differences although the results should remain qualitatively the same.

This atmospheric model is coupled to a mixed-layer ocean, allowing sea-surface temperatures to respond to external forcings. A gravity wave parameterization is employed in the model in which the temperature and wind fields in each grid box are used to calculate gravity wave effects due to wind shear, convection, and topography. Planetary scale waves are generated by land-ocean contrasts and by the influence of topography. For the runs described here, the mountain drag was set to one quarter the amount used in the original documentation [*Rind et al.*, 1988b, a], a standard modification used in many of our subsequent studies, especially those relating to polar ozone [*Shindell et al.*, 1997, 1998a, b, 1999a]. The altered model now gives a good reproduction of observed temperatures in the polar lower stratosphere of each hemisphere during their respective winters and springs. As in the original control simulations [*Rind et al.*, 1988b, a], the residual circulation and the generation of planetary waves in the altered model are in fairly good agreement with observations. Reducing the drag does marginally reduce the variability in the model, as well as slightly degrading the simulation at other seasons and latitudes, however.

The model was run with increasing greenhouse gases starting in 1959, about the earliest time we have good quality global data with which to initialize the model, and extending for 110 years. Given that greenhouse gas increases began much earlier, the model will lack the unrealized warming caused by those earlier emissions (the "cold start" problem), and will therefore slightly underestimate the impact of increasing greenhouse gases. Greenhouse gas trends were based on observations through 1985, and subsequently followed IPCC projections [*Houghton et al.*, 1992]. Five versions of this run were completed, a control run without greenhouse gas increases, and four experimental runs. Three of the experimental runs included additional changes: one included changes in polar lower stratospheric ozone, as in *Shindell et al.* [1998a, 1999a], while the second and third both had changes in stratospheric ozone outside the polar regions, with the third also including positive trends in stratospheric water vapor amounts, which affects both temperatures and stratospheric ozone chemistry [*Shindell*, 2000].

To test the impact of volcanic aerosol perturbations on climate variability patterns, we ran the model again from 1959 to 2000 with increasing greenhouse gases, and also including stratospheric aerosol loading based on observations [*Sato et al.*, 1993, updated through 1999]. The opacity of the volcanic aerosols varied as a function of time; winters with an opacity greater than .02 were deemed volcanic years (1964–66, 1969–70, 1975, 1983–85, 1991–94, mean opacity = .040), while years with a lower opacity were considered background (non-volcanic) years (1959–60, 1967–68, 1971–74, 1976–82, 1986–90, 1995–2000, mean opacity = .009). Both the volcanic and background years are centered around 1979, so that the difference between the average response of the two sets should reflect only the volcanic forcing, and not the influence of the changing greenhouse gases over time. Secondary interactions between ozone and volcanic aerosols are not included in this simulation, though the aerosols do influence local temperatures. Note that the peak opacity after major eruptions can be quite large, with large variations from eruption to eruption: for example, after El Chichon it was about 15 times larger than the mean opacity of the non-volcanic years, and after Mt. Pinatubo it was roughly 25 times larger. Use of many volcanic years allows us to improve the statistical power of our analysis.

Severe ozone depletion in the polar regions, 'ozone holes', were introduced into the climate model using an interactive parameterization of the relevant chemistry, as described previously [*Shindell et al.*, 1997]. In brief, chlorine activation (conversion from reservoir to reactive molecules) is calculated in each model grid box. Complete activation takes place in five hours, based on a simple activation switch triggered whenever temperatures fall below 195°K, a rough threshold for polar stratospheric cloud (PSC) or supercooled ternary solution (STS) formation. This simple activation switch gives reasonable results since the heterogeneous reactions that activate chlorine are very rapid even for very small surface areas. When heterogeneous processing ceases, deactivation follows two-

dimensional model derived rates. Ozone depletion takes place at each point in the GCM where there is both active chlorine and sunlight, which is required for the chlorine catalytic cycle of ozone destruction. We also include an additional estimated contribution to halogen catalyzed ozone depletion of 15% from bromine, as calculated in the offline chemical model. Ozone recovery rates are parameterized so that ozone losses are restored based on the photochemical lifetime of ozone at each altitude. This parameterization has been shown to yield a good reproduction of observed levels of ozone depletion in both hemispheres during the 1980s and 1990s [*Shindell et al.*, 1997, 1998a, b]. This model was run for 19 years with no changes in external forcing, and total chlorine set to 3.2 parts per billion by volume (ppbv), corresponding to early 1990s abundances.

While long-term changes in solar irradiance have certainly influenced the stratosphere, they are not well constrained due to the lack of observations. The roughly 11-year solar cycle has been well observed however, so we have investigated its impact in our model [e.g. *Balachandran and Rind*, 1995; *Rind and Balachandran*, 1995; *Shindell et al.*, 1999b]. The atmosphere's response to longer-term solar output variability would perhaps be similar, though this could be affected by the longer time scale of the forcing or by differences in the spectrum of irradiance variability. One should keep in mind that there is also no guarantee that non-linear changes in atmospheric circulation would extrapolate linearly to longer-term solar changes. The simulations analyzed here include realistic wavelength-dependent solar cycle irradiance changes from 180 to 400 nm, and constant changes at longer wavelengths consistent with total solar cycle irradiance variations [*Lean et al.*, 1997]. We also includes an interactively calculated ozone response to those changes. The ozone response is based on a two-dimensional model-derived chemistry parameterization which includes wavelength-dependent ozone response to changes in radiation and response to changes in temperature [*Shindell et al.*, 1999b]. Solar variability directly affects both ozone photochemistry and local heating, modifying ozone abundances, which in turn further alter local heating rates, as well as the radiation field at other levels. The GCM was run for 20 years each at constant solar maximum and solar minimum conditions to get reasonable statistics on each phase of the solar cycle. Since either phase would not actually persist continually for so long, sea-surface temperatures were held fixed in these runs so as not to yield a false response.

Most calculations of the climate response to anthropogenic greenhouse gas forcing have been based upon tropospheric models with limited stratospheric resolution, and a highly damped or truncated stratospheric circulation. For comparison with the stratospheric model, we have examined simulations with a tropospheric model having the same $8° \times 10°$ horizontal resolution and physics (model II) [*Hansen et al.*, 1983], and a newer version with $4° \times 5°$ horizontal resolution and several improvements in model physics (model II') as discussed or referenced in *Rind and Lerner* [1996]. Both versions have 9 vertical layers, with only 1 or 2 layers in the stratosphere (depending upon latitude). A simulation with a version of model II' containing an interactive simulation of sulfate chemistry has been analyzed as well [*Koch et al.*, 1999]. Lastly, we have also examined the behavior of a coupled ocean-atmosphere version of the model [*Russell et al.*, 2000]. Both versions of the atmospheric GCM, as well as the coupled model, have been run with increased greenhouse gas forcing as for the stratospheric model. For sulfate, we examine the climate response to anthropogenic sulfate increases by looking at the difference between a run with present day sulfate and one with pre-industrial values [*Koch et al.*, 1999].

We point out that 650 years in total were simulated with the stratospheric model, reemphasizing why we were forced to use a coarse resolution model

3. Analysis

Empirical Orthogonal Functions (EOFs) were calculated from the NH cold season (Nov-Apr) SLP time series of the control run. The trend from the transient greenhouse gas runs was then projected upon those EOFs. (However, since the spatial pattern of the leading mode of SLP variability is a robust feature resembling the AO in each simulation, we would have obtained similar results using each simulations own leading mode, as in *Shindell et al.* [1999a]). Other forcings were not run as transients, so differences between two states are used. For the solar cycle variability simulations, the difference between the runs with solar maximum and solar minimum conditions was used. For the volcanic forcing, the difference between the years when stratospheric aerosol loading was large - primarily the few years immediately following eruptions - and years with background levels was used. Results for the ozone hole simulations are

differences between the simulation with polar heterogeneous chemistry included and a control run without the chemistry parameterization. For the transient simulations, we define the time series corresponding to the leading EOF as the 'index' of the model's AO. The spatial pattern has been normalized so that the value of the AO index is equal to the SLP anomaly averaged poleward of 60°N, and is given in mbar. For the transient runs, the AO index trend is given over a thirty year period to match the observational record. For the stratospheric model, this is the period after initial spin up, which requires roughly 20 years for the ocean to fully respond to atmospheric forcing, and before an apparent saturation (see discussion below). While this does not match exactly in time with the observational period, as our models runs began in 1959, so spin-up was completed only in 1979, it seems to be the most realistic period for comparison, as the real world does not have an initial 'cold start' problem. If we were to compare the same 1967–1997 period with the observations, the model's trend would be reduced by about 1/3, but is still much larger than that seen in the tropospheric models (as is true for the entire run length, as shown in *Shindell et al.* [1999a]). The three-decade value we present here was consistent for the entire five decades during which the AO increased steadily between the initial spinup and eventual saturation. For the tropospheric runs, the averaging period has a minimal effect on the results, as the trends were so small that no saturation was seen. For the solar, volcanic, and ozone hole simulations, whose results are differences, we obtain a single value for the change in the AO index based upon the component of the total SLP difference associated with the AO.

While the leading EOF is well separated from subsequent patterns, the higher EOFs are not adequately distinct from one another. In the stratospheric model forced with increasing greenhouse gases, EOF 1 accounts for 13.3% of the variance, but subsequent EOFs account for 5.9, 4.8, 4.1, and 3.5%, respectively, which are not statistically different within the calculated variance range of about 2% (calculations based on the entire 110 year run). An EOF analysis of the observations yields similar results, with 21.3, 11.7, 11.1, 8.2, and 7.0% variance explained by the first five EOFs (calculations based on 1947–1997 data). Again, only the leading pattern is well-separated from the others. Since the higher modes are mathematical constructs which are forced to be orthogonal to the leading mode, not well separated, and lacking an obvious physical interpretation, we restrict our analysis to the leading EOF (the AO).

As discussed in *Shindell et al.* [1999a], the version of the GISS model containing a realistic representation of stratospheric processes produces an increasing AO trend in response to greenhouse gas increases of ≈0.8 mb/decade during the several decades between spin-up and saturation during which the AO index is increasing steadily. This value is comparable to the roughly 1 mb/decade suggested by observations in recent decades. In contrast, model versions lacking a realistic stratosphere, 'tropospheric models' with only 1 or 2 layers in the stratosphere, produce a leading EOF that also looks very much like the AO, but its index shows only a weak increasing trend (+0.1–0.3 mb/decade) which is not statistically significant (Figure 3). It is interesting that when stratospheric water vapor is allowed to increase steadily, as a result of tropopause warming and methane oxidation [*Shindell*, 2000], this distinction between stratospheric and tropospheric models is slightly reduced. When water vapor and greenhouse gases both increase, the AO trend is reduced to ≈0.6 mb/decade, outside the range of the trend in the other three increasing greenhouse gas simulations (0.83, 0.78, and 0.79). This is due to the slight decrease in the meridional temperature gradient that results from mid-latitude cooling that ensues from water vapor induced ozone destruction in the lower stratosphere [*Shindell*, 2000]. Those simulations do not include the potential effect of increased water vapor on heterogeneous ozone destruction in the polar region, however, which would oppose the mid-latitude ozone induced cooling and could potentially cause a significant increase in the meridional temperature gradient in the spring (see section 5.2 below). Water vapor on its own, as a greenhouse gas, increases the bias towards the high phase of the AO.

We find that the inclusion of an ozone hole in the model, another candidate for driving the observed increases [e.g. *Graf et al.*, 1998; *Volodin and Galin*, 1999], does cause an increase in the model's AO index, but of only ≈0.6 mb (1990s ozone depletion relative to the 1970s and earlier, when there was no depletion, or approximately 0.3 mb/decade over the past two decades). Though this has likely contributed to the measured trend, it seems insufficient to account for a great deal of the observed increase of several mbar over the past three decades. This is perhaps not surprising, since the trend in the AO has been observed throughout the November-to-April cold season, but severe ozone depletion in the Arctic does not take place in general until the spring, when sunlight falls

on cold vortex air. These results are consistent with our earlier conclusion that the addition of ozone depletion to greenhouse gas forcing was not required to induce a trend in the AO [*Shindell et al.*, 1999a]. This conclusion is also in agreement with the mild increase in the wintertime meridional temperature gradient at Northern high latitudes calculated based upon TOMS ozone trends [e.g. *Ramaswamy et al.*, 1996]. While the TOMS observations were extrapolated to high latitudes during the polar night, the use of in situ ozonesonde data [*Randel and Wu*, 1999a] does not change this conclusion [*Rosier and Shine*, 2000]. This contrasts with the situation in the Antarctic, where ozone depletion seems to account for nearly the entirety of the observed temperature trends [*Randel and Wu*, 1999b].

Volcanic forcing can be strong in the years immediately following an eruption, leading to an AO difference of 0.4 mb between volcanic and non-volcanic years, but since it is an intermittent forcing that decays rapidly, it also seems unlikely to have contributed greatly to the long-term observed trend. Solar cycle variability causes an increase in the AO index of 0.3 mb between solar maximum and minimum. Since the longer-term trend in irradiance over the past 30 years has been of comparable size to solar cycle variability, it also seems unlikely that solar variability has been responsible for much of the observed trend. Furthermore, estimated solar irradiance increased as much in the first half of the 20th century as in the second [*Lean et al.*, 1997], but the AO index showed no increase during the former. Note that solar irradiance over the satellite period is much better know than earlier.

The stratosphere model is distinct from the tropospheric models not only for exhibiting a trend of magnitude comparable to the observed value, but because the spatial distribution of its SLP trend closely resembles the AO spatial pattern, as observed [*Thompson and Wallace*, 1998]. The resemblance of the SLP trend to the AO spatial pattern can be quantified by decomposing the trend into the EOFs of SLP, and measuring the contribution of each EOF to the trend variance (Figure 2), following *Fyfe et al.* [1999]. The trend in observations of cold season SLP between 1947 and 1997 [*Trenberth and Paolino*, 1980, updated to 1997] is dominated by a change in the AO (the leading EOF), which contributes 56% of the trend. The GISS stratospheric model with increasing greenhouse gases puts 64% of the trend in the AO (the average value of the ensemble of four simulations). The stratospheric model with either an ozone hole or volcanic forcing also projects primarily onto the first EOF, however solar cycle variability does not. The stratospheric model with increasing water vapor projects less strongly onto the AO than do the other increasing greenhouse gas runs, but its trend is still dominated by the AO (and actually looks most like the observed trend projections).

In contrast, GISS model versions lacking a detailed stratosphere - 'tropospheric models' - forced with increasing greenhouse gases produce trends that project only 5-20% onto the AO (Figure 2). The GISS tropospheric model including sulfate aerosols puts just 6% of its trend into the leading EOF, with most of its trend spread out over a large number of patterns. Transient greenhouse gas experiments by other modeling groups seem to be consistent with this distinction (Figure 2). The Canadian Climate Center CCCma model [*Fyfe et al.*, 1999], which shows a positive AO trend in response to increasing greenhouse gases despite the absence of detailed stratospheric dynamics, similarly fails to reproduce the observed dominance of the AO pattern, putting less than 30% of its total trend into its leading EOF. A Geophysical Fluid Dynamics Laboratory (GFDL) climate model version lacking a detailed stratosphere also finds that the majority of its SLP trend in response to increasing greenhouse gases is not in the AO (Paul Kushner, personal communication). Several other groups have presented the simulated AO response to increasing greenhouse gases. The ECHAM3 model from the Max Planck Institute for Meteorology, without a full representation of the stratosphere, shows a systematic increase in the AO index in response to increasing greenhouse gases [*Graf et al.*, 1995, 1998; *Perlwitz et al.*, 2000], but its amplitude is stated to be weaker than observed. *Paeth et al.* [1999] present results of simulations with both the ECHAM3 and ECHAM4 models (showing NAO trends, but these are likely very similar to AO trends). *Zorita and Gonzalez-Rouco* [2000] present the AO trends from the same simulations, adding in results from the Hadley Center model 2 as well. Along with *Fyfe et al.* [1999], all of these groups use normalized units to present their trends, making it impossible to compare the magnitude of the increase in those simulations to the observed value. We suggest that documentation of a model's AO trend should include, at minimum: (1) the trend's magnitude in mb and its statistical significance, with a description of the area weighting used, and (2) the decomposition of the trend into its com-

ponent EOFs. This information would facilitate a comparison across models to document more clearly the role of stratospheric dynamics. As yet, only models that realistically simulate the stratosphere have quantitatively demonstrated an AO trend of roughly the right magnitude and with the same predominance within the SLP trend as the observations

4. Impacts

Strong trends in surface winds over the North Atlantic are closely correlated with the AO, which has the largest effect in this sector. Figure 4 shows trends in zonal wind speed from the NCEP reanalysis data set [*Kalnay et al.*, 1996] and from various GISS models. Clearly the stratospheric model is best able to simulate the observed increase in westerly flow (note that like many climate change signals, this one is just beginning to emerge from an extremely variable pattern). The consequences are visible downstream over Siberia, where an increase in warm oceanic air carried from the Atlantic leads to a rise in surface air temperatures. Again, the stratospheric model is best able to reproduce the observed changes (Figure 5 - see also *Shindell et al.* [1999a]).

Another region of great interest is the area around Labrador and Newfoundland, where surface temperatures have been decreasing over recent decades. Surface wind changes in this region include a significant meridional component, which is associated with altered planetary wave propagation, in addition to the strengthened westerlies discussed above. In the tropospheric model, this region warms significantly as greenhouse gases increase (Figure 6). The stratospheric model, with an increased AO bringing more cool, continental air to the Eastern edge of North America, does a better job, with much less warming, but still does not capture the observed cooling trend. In this region, the use of a coupled, dynamic ocean makes a considerable difference, however, as shown in Figure 6. The tropospheric model coupled to a dynamic ocean model [*Russell et al.*, 2000] does a much better job than the tropospheric model run with a simple mixed-layer ocean. This may indicate that both the stratosphere and the ocean play important roles in bringing about the cooling seen in this region. Additionally, the tropospheric model, using fixed sea-surface temperatures, also does a better job when sulfate aerosol changes are incorporated, though the ones included here are pre-industrial versus present-day, and so much larger than the changes over the past few decades alone

5. Physical Mechanism

5.1 Effect of increasing greenhouse gases

The radiative impact of greenhouse gases at a particular location depends upon the ratio of the absorption of upwelling longwave radiation and the emission of radiation by the molecules. Since absorption and emission depend upon the fourth power of temperature, the net balance will be determined by differences between the mean temperature at which the upwelling radiation was emitted and the local temperature at which the greenhouse gases are emitting. This leads to opposing radiative effects in the troposphere and stratosphere. In the troposphere, the lapse rate is positive (temperature decreasing with altitude), so that molecules emit less radiation than they receive, leading to a net warming. In the stratosphere, the lapse rate is negative, leading to net cooling. Because the height of the tropopause, which separates these two layers, is higher at low latitudes due to vertical mixing, and decreases abruptly poleward of the mid-latitude jet, increasing greenhouse gases will enhance the meridional temperature gradient across the jet core. This gradient, which is largely zonally symmetric, is associated with strengthened westerlies within the jet. The strengthened mid-latitude jet alters the propagation of planetary waves, which can potentially feed back on the jet through eddy forcing.

Any amplification effect would be largest in Northern Hemisphere winter, when planetary wave activity is greatest. While we used the November-April cold-season for SLP, to facilitate comparison with other analyses of the AO, we return now to the conventional December-February winter period for easier comparison with model output and with observations of more standard meteorological parameters. In that season, the enhanced polar night jet strengthens the polar vortex over the Arctic [*Shindell et al.*, 1998a; *Rind et al.*, 1998]. Planetary wave refraction is governed by wind shear, among other factors, so that enhanced wave refraction occurs as the waves approach the area of increased wind. In this case, since planetary waves are propagating up from the surface, they are refracted by the increased vertical shear below the enhanced zonal wind. Equatorward refraction of planetary waves at the lower edge of the wind anomaly (Figure 7) leads to wave divergence and hence an acceleration of the zonal wind in that region. Over time, the wind anomaly itself thus propagates downward

[*Haynes et al.*, 1991] from the lower stratosphere to the surface.

The precise location of the enhanced westerlies shown in Figure 7 therefore depends upon the interaction between planetary waves, wind shears, eddy fluxes and angular momentum fluxes, and is not a simple function of the location of the strongest temperature contrast. This is likely the cause of the difference in location between the strongest enhancement of the temperature gradient, which is at the latitude of the jet stream, and the location of the strongest zonal wind enhancement, which is at the latitude of the polar night jet. Further work will be required to fully elucidate the link between the meridional structures of the temperature and wind responses to external forcing.

Observations suggest that the Arctic vortex has indeed strengthened recently [*Tanaka et al.*, 1996; *Zurek et al.*, 1996; *Waugh et al.*, 1999; *Hood et al.*, 1999]. Likewise, a trend towards equatorward wave fluxes and downward propagation of wind anomalies is also seen in observations [*Kodera and Koide*, 1997; *Kuroda and Kodera*, 1999; *Ohhashi and Yamazaki*, 1999; *Baldwin and Dunkerton*, 1999; *Hartmann et al.*, 2000]. Other model simulations show qualitatively similar effects on planetary wave propagation [*Kodera et al.*, 1996; *Perlwitz et al.*, 2000].

The overall equatorward refraction of planetary waves and reduced upward propagation at high latitudes shown in Figure 7 affects the location of wave dissipation. The net result is a reduced ability of individual waves to abruptly enhance the residual circulation and create sudden warmings. In fact, there is a strong anti-correlation between the frequency of sudden stratospheric warmings and the AO index strength [*Hartmann et al.*, 2000].

The behavior of the troposphere is in accord with theory stating that angular momentum is in general transported in the opposite meridional direction to planetary wave energy [*Andrews et al.*, 1987]. In this case, angular momentum is then preferentially transported poleward, enhancing westerlies, as waves are refracted towards the equator in the upper troposphere. Geostrophic and hydrostatic balance in the atmosphere is maintained by generation of a vertical circulation cell consistent with the northerly angular momentum transfer. Increased westerlies are transformed into northerly flow by surface friction, leading to a cell with rising air in the polar region, and descending air at middle latitudes from about 40°to 55°N throughout the troposphere and the lower stratosphere. The effects are clearly visible in the sea-level pressure field as a decrease in the Arctic concurrent with increased mid-latitude pressure. Adiabatic expansion of rising air at high latitudes must be balanced by radiative heating, which occurs as a result of further cooling of the air below its radiative equilibrium temperature. Conversely, sinking air at mid-latitudes warms. The increased latitudinal temperature gradient that results is consistent with the increased westerly zonal wind around 55°N seen in the model and in observations [*Baldwin and Dunkerton*, 1999; *Thompson et al.*, 2000]. The surface wind anomaly is therefore created by the effect of the increased lower stratospheric zonal wind on planetary waves via linked changes in planetary wave and angular momentum fluxes. It is this increase in surface wind that leads to greater advection of warm oceanic air over the downstream continents. The role of the stratosphere in influencing the behavior of surface meteorology in the model is in agreement with the observed co-variability between the lower stratosphere and the surface [e.g. *Perlwitz and Graf*, 1995; *Graf et al.*, 1995; *Thompson and Wallace*, 1998]. It is also consistent with the large role played by planetary waves in creating the AO pattern itself during mid-winter in the Northern Hemisphere, as evidenced by the fact that the AO structure amplifies with height up into stratosphere only during this season, when the zonal flow is conducive to strong wave-mean flow interaction [*Baldwin and Dunkerton*, 1999; *Thompson and Wallace*, 2000]. This would also explain why there has only been an upward trend in the AO during

Northern Hemisphere winter. Circulation changes arise as a result of the approximately zonally symmetric thermal gradient changes caused by increasing greenhouse gases. Planetary wave propagation is a secondary response to those changes. Since the initial forcing is zonally symmetric, it is perhaps not surprising that the response is composed primarily of an enhancement of the largely zonally symmetric AO pattern. Within this pattern, however, there are some longitudinal variations as the centers of wave activity are typically downstream of wave generating coastlines and mountain ranges. The strongest component of the mid-latitude SLP variability is over the North Atlantic (the much studied North Atlantic Oscillation [e.g. *Hurrell*, 1995]. Longitudinal variations in the model can best be seen by examining the driving force for the SLP changes, the middle troposphere wave activity flux for stationary planetary waves [*Plumb*, 1985]. The model has its max-

imum meridional changes occurring over the North Atlantic, where there is a distinct equatorward shift in wave activity around 500mb (Figure 8), similar to the observed change in this sector [*Kodera et al.*, 1996; *Ohhashi and Yamazaki*, 1999]. This shift has been shown to be tied to the AO pattern in other models as well [*Limpasuvan and Hartmann*, 1999].

The equatorward movement of the flux convergence zone allows westerly flow in the northernmost Atlantic to proceed more rapidly, while impeding flow at more southerly latitudes. Similar correlations between flow across the North Atlantic and the strength of the AO (or NAO) are present in observations [*Hurrell*, 1995; *Baldwin and Dunkerton*, 1999], and indicate a preference for storms to follow the more northerly track during the high phase of the AO. This shift persists throughout the winter, leading to a strong reduction in the energy convergence in the region from Iceland to Scandinavia and down through the North Sea, which is typically a strong convergence zone. Reduced wave energy convergence here allows the westerly zonal wind to increase significantly, and therefore plays a large role in the downstream warming effects over the Eurasian continent. Over East Asia and the Western Pacific, there is a westward translation of the wave energy convergence/divergence pattern, a meridional banded structure to begin with. Such a rotation, of course, has little impact on the zonal average zonal flow. There is also a small southerly component to the energy convergence shift over the Western Pacific. Overall then, there is a tendency toward increased wave energy propagation away from the pole, as expected from the increased winds induced by the thermal gradient. This conforms to the generation of an AO type response, with SLP decreases in the polar region, and increases at middle latitudes, especially over the Atlantic and to a lesser extent, the Pacific. It is also consistent with a response pattern that is largely zonally symmetric being created in response to a zonally symmetric thermal gradient increase

5.2 Effect of Arctic ozone depletion

The depletion of ozone in the Arctic region occurs during spring when sunlight returns to the polar region. Ozone depletion takes place extremely rapidly, so that very soon after depletion has begun temperatures in the lower stratosphere show significant decreases, as there is less ozone to absorb solar ultraviolet radiation [*Randel and Wu*, 1999b]. The cooling of the polar lower stratosphere from ozone depletion results in a meridional temperature gradient increase, as in the case of increasing greenhouse gases. The effects on planetary wave propagation are qualitatively almost identical to those seen in the greenhouse gas simulations (Figure 7). The mechanism by which Arctic ozone depletion induces an increased AO is thus basically identical to that of the increasing greenhouse gases, so it is not surprising that the two trends both project primarily onto the AO pattern (Figure 2). However, the Northern Hemisphere ozone depletion occurs primarily during late February, March and April, so that the effect averaged over the entire cold-season is much weaker than that induced by the greenhouse gases (Figure 2). The primary effect of severe ozone depletion on the polar vortex is to make it more persistent into the spring [*Graf et al.*, 1998].

While there is a relatively steady increase in the cold-season averaged strength of the Arctic vortex, as shown by the trend in the 30 mb geopotential height field, ozone depletion remains quite variable during the next four decades since it depends primarily on the vortex strength only during spring (Figure 9). Nevertheless, the trend towards a stronger vortex in the model does lead to significantly enhanced ozone depletion relative to what would occur in the absence of climate change. This is clearly seen in Figure 9, which shows that the maximum predicted ozone losses take place well after the maximum abundances of ozone-destroying halogens are present in the stratosphere.

The ozone recovery trend is fairly constant after about 2020 (middle panel), and the increase in the AO index also levels off at this time (Figure 3b). The vortex, however, continues to strengthen, as shown by the geopotential height field (top panel). A closer examination of the height index shows a slowdown in the rate of increase after about 2020. The saturation seen in the surface AO trends, which are transmitted downwards by increased planetary wave divergence, at around the same time is indicative of the reduced influence of planetary wave propagation changes after about 2020 in the GCM (note that since there are still stratospheric warmings taking place in later decades, as demonstrated by the large variability in ozone loss shown in Figure 9, it is not obvious why the surface trends and planetary wave changes do saturate). The continued increase in the strength of the vortex thereafter is therefore likely driven primarily by the radiative impact of the greenhouse gases. The continued strengthening of the polar vortex aloft im-

plies that the ozone depletion that takes place in the mid-21st century will persist later into the spring than it would have in the absence of increasing greenhouse gases. This effect is overshadowed by the influence of the ozone recovery itself on the persistence of the vortex [e.g. *Zhou et al.*, 2000], through its feedback on temperatures, however. This latter effect dominates the overall persistence, so that the vortex lasts longer and longer into the spring as ozone depletion increases through about 2020, reaching a maximum of about two to three weeks delay in the final warming, but then its duration is slowly reduced from about 2020 to 2040. After this time, it slowly begins to last longer again as ozone depletion in the Arctic is minimal, while greenhouse gases continue to increase

5.3 Effects of solar cycle variability

Solar variability impacts the atmosphere initially by inducing a thermal gradient in the upper stratosphere [*Shindell et al.*, 1999b]. In that region, increased UV radiation at solar maximum relative to solar minimum enhances the photochemical production of ozone in sunlit areas. Heating in these altitudes is due primarily to ozone absorption of UV radiation. Since there is both more UV and more ozone, there is more heating in sunlit areas at solar maximum than minimum. In the wintertime, the polar region is in total darkness, so temperatures there do not change with solar irradiance variations. Thus a latitudinal temperature gradient and a zonal wind anomaly are induced in the upper stratosphere (Figure 10), and again planetary wave propagation is affected. The wind anomaly gradually moves downward [*Kodera et al.*, 1990; *Balachandran and Rind*, 1995; *Rind and Balachandran*, 1995; *Shindell et al.*, 1999b], and as it reaches the lower stratosphere during the middle part of the winter, the resulting horizontal and vertical wind shear changes refract planetary waves equatorward as in the increasing greenhouse gas case. This alters the transport of tropospheric energy, resulting in temperature changes in the lower atmosphere which in turn affect geopotential height, causing significant increases at low and mid-latitudes and decreased heights near the pole [*Shindell et al.*, 1999b]. These height changes are in good agreement with an observational record stretching back more than forty years, and showing a very high level of statistical significance [*Labitzke and van Loon*, 1997], giving credence to the modeled flux and temperature changes (a comparison with other models is given in *Shindell et al.* [1999b]). The zonal mean zonal wind and tropospheric EP flux changes in January in fact look fairly similar to those seen in the increasing greenhouse gas simulations. December and February do not, however (Figure 10), as waves fluxes in the increasing greenhouse gas simulations show little month-to-month change in the upper troposphere/lower stratosphere region.

In contrast to the case of increasing greenhouse gases, the initial temperature changes induced by solar variability take place much higher in the stratosphere. The troposphere sees no direct change in thermal gradients, but instead sees altered planetary wave propagation as the driving force behind changes. It is the changes in wave propagation that lead to the altered temperatures and circulation patterns in the lower stratosphere, as well as in the troposphere. Planetary waves are generated by topography and land-ocean contrasts, so are by nature longitudinally asymmetric. Thus the impact of solar forcing in the lower stratosphere is not as symmetric as that of the greenhouse gases, though the zonal mean changes are at times broadly similar. Stratospheric water vapor also causes large changes in the upper stratosphere [*Shindell*, 2000], and the wave fluxes in the run with increasing water appear to be a combination of those seen in the solar cycle runs and those seen in the greenhouse gas simulations, though primarily the latter.

At solar maximum, averaged winter wave activity flux at 584 mb again shows an overall equatorward shift relative to solar minimum, but in this case, the main activity takes place over the Western Pacific. Over the North Atlantic, there is actually a slight poleward shift in overall wintertime wave energy convergence zones, but the pattern varies strongly over the course of the winter. There is little signal in December, while the February pattern looks the most similar to the greenhouse gas induced pattern, with a slight southerly shift in the North Atlantic energy convergence. Over the Western Pacific, there is a distinct eastward and equatorward shift in wave energy convergence, which is stable during the entire winter and larger than the shift seen in the greenhouse gas runs. This large, more southerly energy propagation is responsible for an overall zonal mean equatorward shift in response to solar cycle forcing [*Shindell et al.*, 1999b], just as in the greenhouse gas simulations' zonal mean responses. This greater wave energy divergence at high latitudes allows the zonal wind to accelerate in that region, creating a strong increase in the westerly flow across the northern-most

Pacific. These results are consistent with a response that begins with a zonally symmetric thermal gradient increase in the upper stratosphere, but that takes place primarily via altered wave propagation once it reaches the lower atmosphere. The centers of activity are therefore downstream from the areas of largest wave activity, i.e. the eastern coasts of Asia and North America (neglecting the orographic forcing from the Himalayas at lower latitudes). The wave energy flux changes affect the downstream synoptic pressure systems as well as the overall westerly flow, so that the response pattern is much less zonally symmetric than with the greenhouse gases. The pattern therefore projects onto many EOFs of sea-level pressure (Figure 2). Note, however, that the use of fixed sea-surface temperatures in these runs may have limited the model's response at the surface.

The increased surface winds in the solar experiment reflect a strengthening of the Pacific subtropical and Azores high pressure systems, and so the increased westerlies over both ocean basins are merely the northward portion of an increased anticyclonic rotation. The impacts on downstream surface warming are significant, as shown in Figure 11. Solar forcing leads to downstream warming at higher latitudes than do greenhouse gases. Differences are especially stark over Asia, where the greenhouse gases lead to a warming over most of the continent north of 45 degrees, but in the solar experiments, the return flow down from the Arctic leads to cooling south of 60 degrees. The influence of using fixed sea-surface temperatures is large, however, so further work in this area will be necessary to obtain more reliable results

5.4 Effect of Volcanic Eruptions

Volcanic forcing induces SLP variations that occur predominantly via the AO pattern, though not as exclusively as in the greenhouse gas experiments or as in the past three decades of observations (Figure 2). The enhanced AO leads to a wintertime continental warming following eruptions, as clearly seen in observations [e.g. *Robock and Mao*, 1995; *Kelly et al.*, 1996]. Changes in wave propagation are quite similar to those seen in the greenhouse gas case, especially in the mid to high latitude troposphere (Figure 12). The injection of stratospheric aerosols causes enhanced absorption of shortwave radiation, leading to heating in the sunlit lower stratosphere [e.g. *Rind et al.*, 1992; *Graf et al.*, 1993]. Along with aerosol-induced longwave cooling at high latitudes, the volcanic forcing thus creates an increased meridional temperature gradient in the lower stratosphere, particularly in winter. This induces a positive zonal wind anomaly, which then leads to equatorward refraction of upward propagating planetary waves. Similar behavior is seen in observations [*Kodera*, 1995]. Note that the magnitude of the AO index response found here, -0.4 mb between volcanic and non-volcanic years, is based on a fairly small average aerosol loading. As noted, the aerosol loading immediately following the eruptions of El Chichon and Mt. Pinatubo were 4 and 6 times larger, respectively, than the 'volcanic years' average used here. The model's AO index increase after these eruptions was much smaller than what a linear extrapolation would yield, implying that saturation effects take place in this forcing as well as in the greenhouse gas forcing.

The importance of the stratosphere to the response seems to be fairly similar in other models. A large set of tropospheric models used in the Atmospheric Model Intercomparison Project (AMIP) could not reproduce the observed wintertime warming over the Northern Hemisphere continents after El Chichon's eruption, which can most likely be attributed to deficiencies in those model's simulation of stratospheric processes [*Mao and Robock*, 1998]. In contrast, models with a somewhat more complete representation of the stratosphere do show an enhanced AO type pattern, as in the GISS stratospheric model, with significant continental surface air temperature increases during wintertime following eruptions [*Kirchner et al.*, 1999; *Robock et al.*, 1999]. It is interesting that a simulation of the response to the eruption of Mt. Pinatubo, using a version of the ECHAM model with a top at 10 mb, does seem to reproduce the observed magnitude of AO enhancement [*Kirchner et al.*, 1999]. (Note that though the model top is in the middle stratosphere at 10 mb, this model nevertheless has a much more realistic stratosphere than the AMIP models). This is likely related to the extremely large forcing of the Pinatubo aerosols, which warmed the lower stratosphere by roughly 3 degrees. This induces a meridional thermal gradient as large as that induced by increasing greenhouse gases over about 50 years. Since the greenhouse gas forcing saturates in the GISS model after increasing for roughly 60 years [*Shindell et al.*, 1999a], presumably as the polar vortex has become strong and stable enough so that nearly all planetary waves are already refracted away, any further forcing is not effective. So while a model with a top at 10 mb might not fully capture alterations in planetary wave propagation, amplifica-

tion of such a large, initial thermal gradient may not be necessary to produce the appropriate response in this particular case

6. Conclusions

A series of general circulation model simulations demonstrate that changes in the stratosphere can influence surface climate. Either anthropogenic or natural perturbations to the stratosphere are capable of causing changes to the stratospheric thermal structure, which in turn affect stratospheric circulation. These wind changes alter the wind shear, affecting propagation of planetary waves out of the troposphere so as to amplify the lower stratospheric wind changes during Northern Hemisphere winter. Furthermore, the deflection of upward propagating waves takes place at steadily lower and lower altitudes, and so exerts a significant impact on surface climate. This fundamental role for planetary waves, which are relatively absent in the Southern Hemisphere, is consistent with studies showing that the radiative impact of ozone depletion is able to account almost completely for observed wintertime temperature trends in the Antarctic, but not in the Arctic [*Randel and Wu*, 1999b].

The model simulations have shown that a surface climate response is induced by increasing greenhouse gases, ozone depletion, volcanic eruptions, and solar variability. Except for solar variability, the others all affect surface climate at Northern Hemisphere middle and high latitudes during winter primarily by favoring the positive phase of the AO, the dominant natural variability pattern, while concurrently strengthening the polar vortex aloft. Nonetheless, only increasing greenhouse gases seem capable of causing an AO trend in our model as large as the observed trend.

Other studies [*Fyfe et al.*, 1999; *Paeth et al.*, 1999; *Zorita and Gonzalez-Rouco*, 2000] note that some models lacking detailed resolution of stratospheric dynamics, exhibit non-zero AO/NAO trends when forced with increasing greenhouse gases. Similar models, such as the ECHAM3 [*Perlwitz et al.*, 2000] and HadCM3 [R. MacDonald, personal communication, 2000] also exhibit non-zero trends that are nonetheless weak compared to the magnitude observed in recent decades. This is consistent with the behavior of the GISS model described above, where only the inclusion of stratospheric dynamics results in an AO trend of magnitude comparable to that suggested by observations in recent decades.

The AO sensitivity of models developed by several groups, including GISS, which lack realistic representations of the stratosphere, is much weaker than the GISS stratospheric model. It seems that models with an overly simplistic stratosphere fail to adequately capture the positive feedback of planetary wave flux changes on circulation anomalies seen in the stratospheric model. Furthermore, the simulated trends in those models are not primarily composed of the AO pattern (with the exception of the ECHAM4/OPYC model, A. Robertson, personal communication, 2000), as are the observations, while the stratospheric model does reproduce this behavior.

We hope that future studies will present quantitative trends of the AO index (along with its statistical significance) for comparison to the observed values and other modeling results (as opposed to the normalized 'AO/NAO' indices), while quantifying the extent to which their trend in SLP resembles the AO spatial pattern. In the meantime, the behavior of the tropospheric models cited above remain in contrast to the GISS stratospheric model. As yet, only the latter has shown an AO trend of roughly the right magnitude and with the same predominance in the SLP trend as the observations. It remains to be demonstrated that a model lacking stratospheric dynamics is able to match both these aspects of the observations.

The surface climate response of the GISS stratospheric model to the injection of volcanic aerosols into the stratosphere corresponds well with observations. This provides important evidence that the modeled linkage between forcings and the AO does indeed occur in the atmosphere. While longer-term AO changes will need to continue for many more years to be fully accepted as a distinct trend, the AO enhancement after eruptions is already quite clear in the observational record. Since the AO responses to greenhouse gas increases, ozone depletion, and volcanic aerosols all take place via the same mechanism, the clearly observed response to large volcanic eruptions suggests that the same linkage is likely at work in the case of the slower, longer-term greenhouse gas and ozone depletion forcings as well.

These results support our earlier conclusion that much of the trend in the AO and in the Arctic vortex strength over the past few decades should be attributed to increasing greenhouse gases, and that the trends are likely to continue.

Acknowledgments. We thank Kunihiko Kodera and Koji Yamazaki for graciously providing the data for ob-

served trends in wave fluxes and zonal winds, and Jim Hansen for surface temperature data. Three anonymous reviewers provided helpful comments on this manuscript. Stratospheric modeling at GISS is supported by NASA's Atmospheric Chemistry Modeling and Analysis Program. RLM was supported by the NOAA Atlantic Climate Change Program. GAS and DTS acknowledge the support of NSF ATM-00-02267.

References

Andrews, D. G., J. R. Holton, and C. B. Leovy, *Middle atmosphere dynamics*, Academic Press, Orlando, 1987.

Balachandran, N. K., and D. Rind, Modeling the effects of UV variability and the QBO on the troposphere-stratosphere system.part i: The middle atmosphere, *J. Clim.*, *8*, 2058–2079, 1995.

Baldwin, M. P., and T. J. Dunkerton, Propagation of the Arctic Oscillation from the stratosphere to the troposphere, *J. Geophys. Res.*, *104*, 30,937–30,946, 1999.

Fyfe, J. C., G. J. Boer, and G. M. Flato, The Arctic and Antarctic Oscillations and their projected changes under global warming, *GRL*, *26*, 1601–1604, 1999.

Graf, H.-F., I. Kirchner, A. Robock, and I. Schult, Pinatubo eruption winter climate effects: Model versus observations, *Clim. Dyn.*, *9*, 81–93, 1993.

Graf, H.-F., J. Perlwitz, I. Kirchner, and I. Schult, Recent Northern winter climate trends, ozone changes and increased greenhouse gas forcing, *Beitr. Phys. Atm.*, *68*, 233–248, 1995.

Graf, H.-F., I. Kirchner, and J. Perlwitz, Changing lower stratospheric circulation: The role of ozone and greenhousegases, *J. Geophys. Res.*, *103*, 11,251–11,261, 1998.

Haigh, J. D., The impact of solar variability on climate, *Science*, *272*, 981–984, 1996.

Haigh, J. D., A GCM study of climate change in response to the 11-year solar cycle, *Q. J. R. Met. Soc.*, *125*, 871–892, 1999.

Hansen, J., R. Ruedy, J. Glascoe, and M. Sato, GISS analysis of surface temperature change, *J. Geophys. Res.*, 1999, (in press).

Hansen, J. E., G. L. Russell, D. Rind, P. Stone, A. Lacis, R. Ruedy, and L. Travis, Efficient three-dimensional models for climatic studies, *Mon. Wea. Rev.*, *111*, 609–662, 1983.

Hartmann, D. L., J. M. Wallace, v. Limpasuvan, D. W. J. Thompson, and J. R. Holton, Can ozone depletion and global warming interact to produce rapid climate change?, *Proc. Natl. Ac. Sci.*, *97*, 1412–1417, 2000.

Haynes, P. H., C. J. Marks, M. E. McIntyre, T. G. Shepherd, and K. P. Shine, On the "downward control" of extratropical diabatic circulation by eddy-induced mean zonal forces, *J. Atmos. Sci.*, *48*, 651–678, 1991.

Hood, L., S. Rossi, and M. Beulen, Trends in lower stratospheric zonal winds, Rossby wave breaking behavior, and column ozone at northern midlatitudes, *J. Geophys. Res.*, *104*, 24,321–24,339, 1999.

Houghton, J. T., B. A. Callander, and S. K. Varney, *Climate Change 1992: The supplementary report to the IPCC Scientific Assessment*, Cambridge Univ. Press, New York, 1992.

Hurrell, J. W., Decadal trends in the North Atlantic Oscillation: Regional temperatures and preipitation, *Science*, *269*, 676–679, 1995.

Kalnay, E., et al., The NCEP/NCAR 40-year reanalysis project, *Bull. Am. Met. Soc.*, *77*, 437–471, 1996.

Kelly, P. M., P. D. Jones, and P. Q. Jia, The spatial response of the climate system to explosive volcanic eruptions, *Int. J. Clim.*, *16*, 537–550, 1996.

Kirchner, I., G. L. Stechnikov, H.-F. Graf, A. Robock, and J. C. Antuna, Climate model simulation of winter warming and summer cooling following the 1991 Mount Pinatubo volcanic eruption, *J.Geophys. Res.*, *104*, 19,039–19,055, 1999.

Koch, D., D. Jacob, I. Tegen, D. Rind, and M. Chin, Tropospheric sulfur simulation and sulfate direct radiative forcing in the Goddard Institute for Space Studies general circulation model, *J. Geophys. Res.*, *104*, 23,799–23,822, 1999.

Kodera, K., Influence of volcanic eruptjons on the troposphere through stratospheric dynamical processes in the northern hemisphere winter, *J. Geophys. Res.*, *99*, 1273–1282, 1994.

Kodera, K., On the origin and nature of the interannual variability of the winter stratospheric circulation in the northern hemisphere, *J. Geophys. Res.*, *100*, 14,077–14,087, 1995.

Kodera, K., and H. Koide, Spatial and seasonal characteristics of recent decadal trends in the northern hemisphere troposphere and stratosphere, *J. Geophys. Res.*, *102*, 19433–19447, 1997.

Kodera, K., K. Yamazaki, M. Chiba, and K. Shibata, Downward propagation of upper stratospheric mean zonal wind perturbation to the troposphere, *Geophys. Res. Lett.*, *17*, 1263–1266, 1990.

Kodera, K., M. Chiba, H. Koide, A. Kitoh, and Y. Nikaidou, Interannual variability of the winter stratosphere and troposphere in the northern hemisphere, *J. Meteorol. Soc. Jpn*, *74*, 365–382, 1996.

Kuroda, Y., and K. Kodera, Role of planetary waves in the stratosphere-troposphere copuled variability in the Northern Hemisphere winter, *Geophys. Res. Lett.*, *26*, 2375–2378, 1999.

Kutzbach, J. E., Large-scale features of monthly mean Northern Hemisphere anomaly maps of sea-level pressure, *Mon. Wea. Rev.*, *98*, 708–716, 1970.

Labitzke, K., and H. van Loon, The signal of the 11-year sunspot cycle in the upper troposphere-lower stratosphere, *Space Sci. Rev.*, *80*, 393–410, 1997.

Lean, J. L., G. Rottman, H. Kyle, T. Woods, J. Hickey, and L. Puga, Detection and parameterization of variations in solar mid and near ultraviolet radiation (200 to

400 nm), *J. Geophys. Res.*, *102*, 29,939–29,956, 1997.

Limpasuvan, V., and D. L. Hartmann, Eddies and the annular modes of climate variability, *Geophys. Res. Lett.*, *26*, 3133–3136, 1999.

Mao, J., and A. Robock, Surface air temperature simulations by AMIP general circulation models: Volcanic and ENSO signals and systematic errors, *J. Clim.*, *11*, 1538–1552, 1998.

Ohhashi, Y., and K. Yamazaki, Variability of the Eurasian pattern and its interpretation by wave activity flux, *J Met. Soc. Japan*, *77*, 495–511, 1999.

Paeth, H., A. Hense, R. Glowienka-Hense, R. Voss, and U. Cubash, The North Atlantic Oscillation as an indicator for greenhouse-gas induced regional climate change, *Clim. Dyn.*, *15*, 953–960, 1999.

Perlwitz, J., and H.-F. Graf, The statistical connection between tropospheric and stratospheric circulation of the northern hemisphere in winter, *J. Clim*, *8*, 2281–2295, 1995.

Perlwitz, J., H.-F. Graf, and R. Voss, The leading variability mode of the coupled troposphere-stratosphere winter circulation in different climate regimes, *J. Geophys. Res.*, *105*, 6915–6926, 2000.

Plumb, R. A., On the three-dimensional propagation of stationary waves, *J. Atmosphere. Sci.*, *42*, 217–229, 1985.

Ramaswamy, V., M. D. Schwarzkopf, and W. J. Randel, Fingerprint of ozone depletion in the spatial and temporal pattern of recent lower-stratospheric cooling, *Nature*, *382*, 616–618, 1996.

Randel, W. J., and F. Wu, A stratospheric ozone trends data set for global modeling studies, *Geophys. Res. Lett.*, *26*, 3089–3092, 1999a.

Randel, W. J., and F. Wu, Cooling of the Arctic and Antarctic polar stratospheres due to ozone depletion, *J. Clim.*, *12*, 1467–1479, 1999b.

Rind, D., and N. K. Balachandran, Modeling the effects of UV variability and the QBO on the troposphere-stratosphere system. Part II: The troposphere, *J. Clim.*, *8*, 2080–2095, 1995.

Rind, D., and J. Lerner, Use of on-line tracers as a diagnostic tool in general circulation model development .1. Horizontal and vertical transport in the troposphere, *J. Geophys. Res.*, *101*, 12,667–12,683, 1996.

Rind, D., R. Suozzo, and N. K. Balachandran, The GISS global climate/middle atmosphere model. Part II: Model variability due to interactions between planetary waves, the mean circulation, and gravity wave drag, *J. Atmos. Sci.*, *45*, 371–386, 1988a.

Rind, D., R. Suozzo, N. K. Balachandran, A. Lacis, and G. Russell, The GISS global climate/middle atmosphere model. Part I: model structure and climatology, *J. Atmos. Sci.*, *45*, 329–370, 1988b.

Rind, D., N. K. Balachandran, and R. Suozzo, Climate change and the middle atmosphere. Part II: The impact of volcanic aerosols, *J. Clim.*, *5*, 189–208, 1992.

Rind, D., D. T. Shindell, P. Lonergan, and N. K. Balachandran, Climate change and the middle atmosphere. Part III: The doubled CO_2 climate revisited, *J. Clim.*, *11*, 876–894, 1998.

Robock, A., and J. Mao, The volcanic signal in surface temperature observations, *J. Clim.*, *8*, 1086–1103, 1995.

Robock, A., G. L. Stechnikov, S. Ramachandran, and V. Ramaswamy, Winter warming following volcanic eruptions: Observations and climate model simulations of forced Arctic Oscillation patterns, *EOS*, *80*, 232, 1999.

Rosier, S. M., and K. P. Shine, The effect of two decades of ozone change on stratospheric temperature as indicated by a general circulation model, *Geophys. Res. Lett.*, 2000, (in press).

Russell, G. L., J. R. Miller, D. H. Rind, R. A. Ruedy, G. A. Schmidt, and S. Sheth, Comparison of model and observed regional temperature changes during the past 40 years, *J. Geophys. Res.*, *105*, 14891–14898, 2000.

Sato, M., J. Hansen, M. McCormick, and J. Pollack, Stratospheric aerosol optical depths, 1850–1990, *J. Geophys. Res.*, *98*, 22,987–22,994, 1993.

Shindell, D. T., Global warming due to increased stratospheric water vapor, *J. Geophys. Res.*, 2000, (in press).

Shindell, D. T., S. Wong, and D. H. Rind, Interannual variability of the Antarctic ozone hole in a GCM. Part 1: The influence of tropospheric wave variability, *J. Atmos. Sci.*, *54*, 2308–2319, 1997.

Shindell, D. T., D. H. Rind, and P. Lonergan, Increased polar stratospheric ozone losses and delayed eventual recovery due to increasing greenhouse gas concentrations, *Nature*, *392*, 589–592, 1998a.

Shindell, D. T., D. H. Rind, and P. Lonergan, Climate change and the middle atmosphere. Part IV: Ozone photochemical response to doubled CO_2, *J. Clim.*, *11*, 895–918, 1998b.

Shindell, D. T., R. L. Miller, G. A. Schmidt, and L. Pandolfo, Simulation of recent northern winter climate trends by greenhouse-gas forcing, *Nature*, *399*, 452–455, 1999a.

Shindell, D. T., D. Rind, N. Balachandran, J. Lean, and P. Lonergan, Solar cycle variability, ozone, and climate, *Science*, *284*, 305–308, 1999b.

Tanaka, H. L., R. Kanohgi, and T. Yasunari, Recent abrupt intensification of the northern polar vortex since 1988, *J. Met.Soc. Japan*, *74*, 947–954, 1996.

Thompson, D. W. J., and J. M. Wallace, The Arctic Oscillation signature in the wintertime geopotential height and temperature fields, *Geophys. Res. Lett*, *25*, 1297–1300, 1998.

Thompson, D. W. J., and J. M. Wallace, Annular modes in the extratropical circulation. Part I: Month-to-month variability, *J. Clim.*, *13*, 1000–1016, 2000.

Thompson, D. W. J., J. M. Wallace, and G. C. Hegerl, Annular modes in the extratropical circulation. Part

II: Trends, *J. Clim.*, *13*, 1018–1036, 2000.

Trenberth, K. E., and D. A. Paolino, The Northern hemisphere sea level pressure data set: Trends, errors and discontinuities, *Monthly Weather Review*, *108*, 855–872, 1980.

Volodin, E. M., and V. Y. Galin, Interpretation of winter warming on Northern Hemisphere continents in 1977-94, *J. Clim.*, *12*, 2947–2955, 1999.

Waugh, D. W., W. J. Randel, S. Pawson, P. A. Newman, and E. R. Nash, Persistence of the lower stratospheric polar vorticies, *J.Geophys. Res.*, *104*, 27,191–27,201, 1999.

World Meteorological Organization, Scientific assessment of ozone depletion: 1998, World Meteorological Organization, Geneva, 1999, Rep. 44.

Zhou, S., M. E. Gelman, A. J. Miller, and J. P. McCormack, An inter-hemisphere comparison of the persistent stratospheric polar vortex, *Geophys. Res. Lett.*, *27*, 1123–1126, 2000.

Zorita, E., and F. Gonzalez-Rouco, Disagreement between predictions of the future behavior of the Arctic Oscillation as simulated in two different climate models: Implications for global warming, *Geophys. Res. Lett.*, *27*, 1755–1758, 2000.

Zurek, R. W., G. L. Manney, A. J. Miller, M. E. Gelman, and R. M. Nagatani, Interannual variability of the north polar vortex in the lower stratosphere during the UARS mission, *Geophys. Res. Lett.*, *23*, 289–292, 1996.

D. T. Shindell, NASA Goddard Institute for Space Studies, 2880 Broadway, New York, NY 10025 (dshindell@giss.nasa.gov)

G. A. Schmidt, NASA Goddard Institute for Space Studies and Center for Climate Systems Research, Columbia University, 2880 Broadway, New York, NY 10025 (gschmidt@giss.nasa.gov)

R. L. Miller, NASA Goddard Institute for Space Studies, 2880 Broadway, New York, NY 10025 (rmiller@giss.nasa.gov)

D. Rind, NASA Goddard Institute for Space Studies, 2880 Broadway, New York, NY 10025 (cddhr@giss.nasa.gov)

Received Feb 15, 2000; revised August 15, 2000

This preprint was prepared with AGU's LaTeX macros v5.01. File ao2 formatted August 22, 2000.

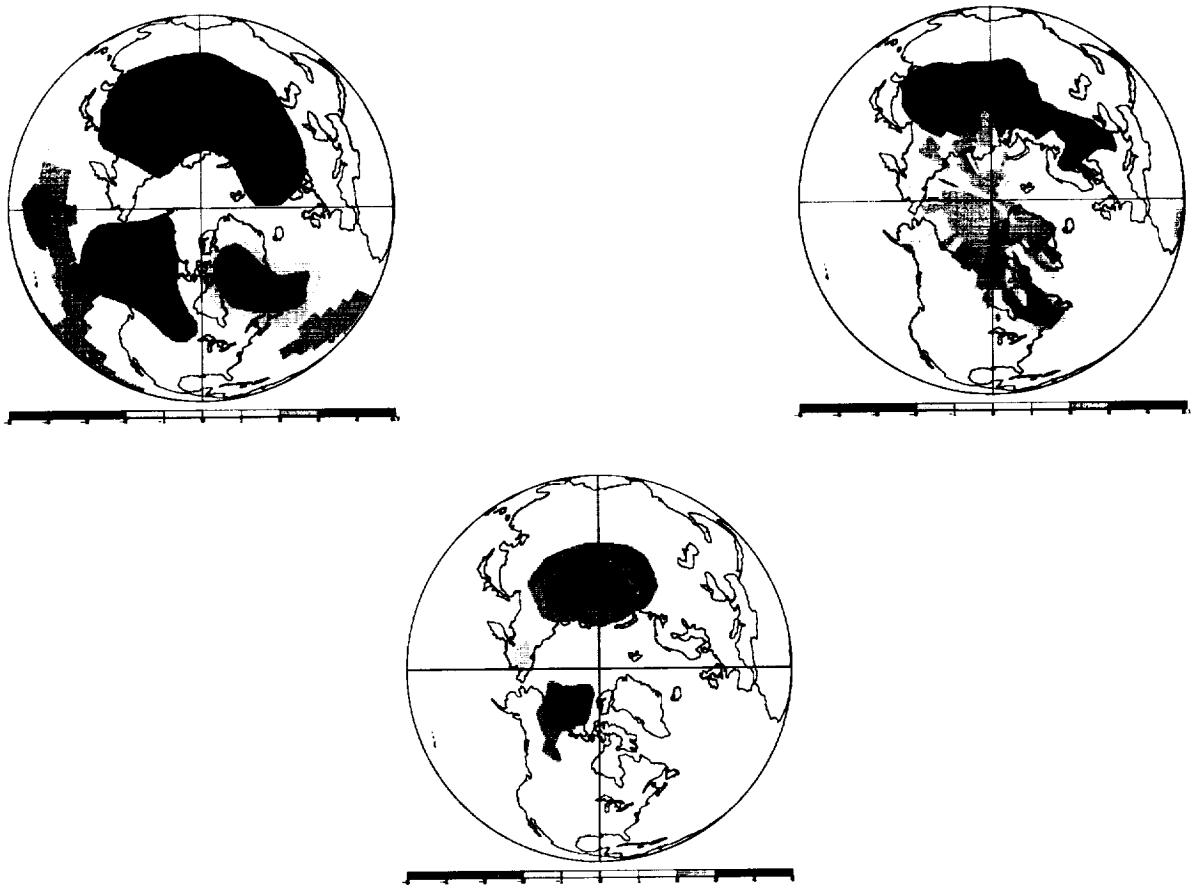

Figure 1. Surface temperature trends (C). Top left: Observed surface temperature trend from 1965 to 1995, December to February average [*Hansen et al.*, 1999]. Top right: The AO contribution to the total trend, obtained by regressing the temperature trend onto the AO spatial pattern as in *Thompson et al.* [2000]. Bottom center: The AO component of the total trend in the GISS stratospheric model, similarly obtained by regressing the model's temperature trend onto its AO spatial pattern. Grey areas are those where no data is present. Note that the difference in grey areas between the top left and top right panels results from the use of slightly different temperature data sets, which do not match exactly in areas with few observations (Arctic Ocean and low latitude Atlantic and Pacific).

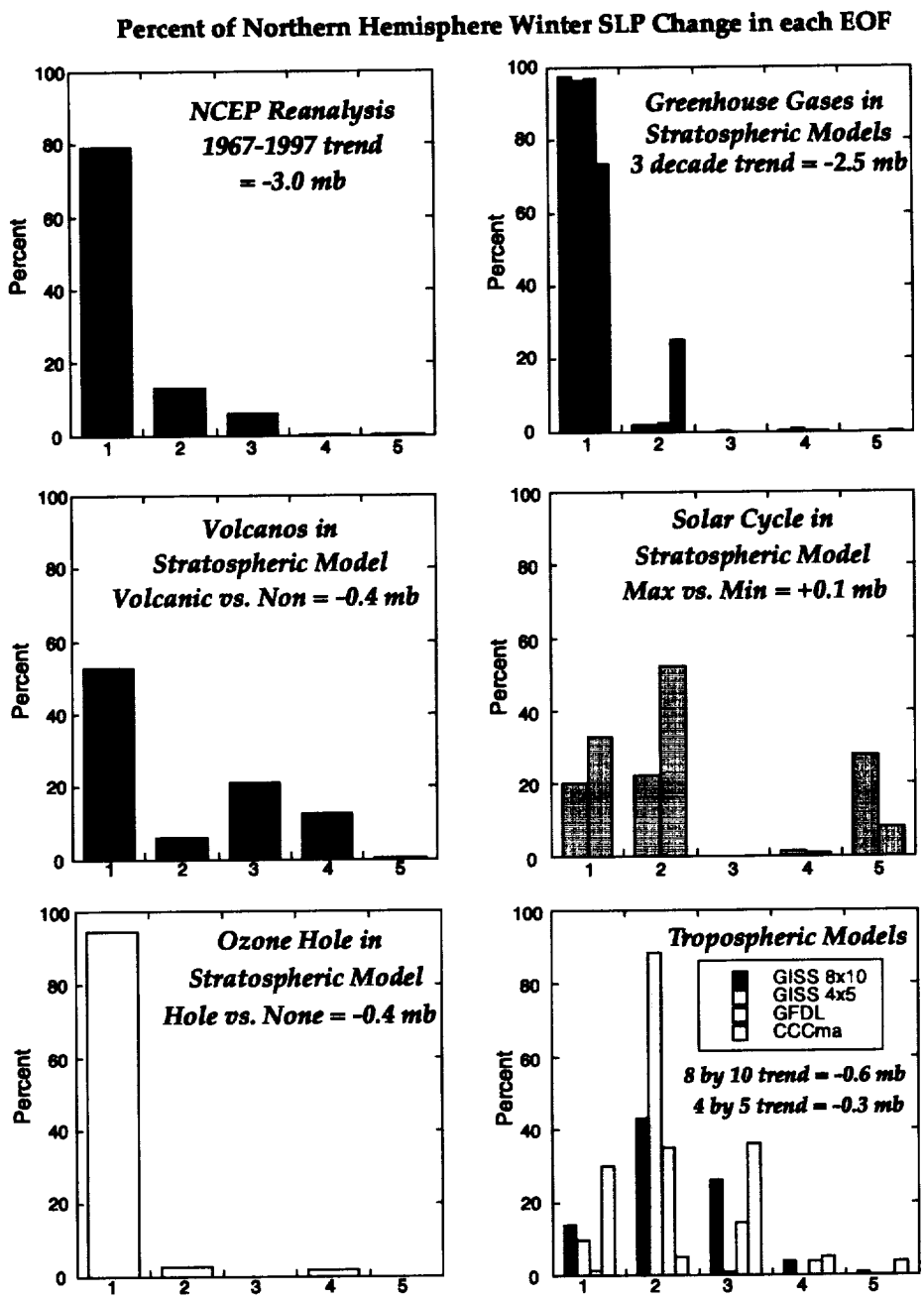

Figure 2. Percentage of the total Northern Hemisphere November-April sea-level pressure change in each EOF. Trends from each indicated model simulation were projected upon the control run EOFs. The magnitude of the trend or change in the AO index induced by each forcing is also given. Values are calculated using a linear least-squares regression through the observations or model output. Uncertainties are given in Table 1, and are 95% confidence limits based on a student's-T test, assuming each winter is independent (Note that assuming red noise instead of white has a minimal effect on these results). Observations are updated from *Trenberth and Paolino* [1980].

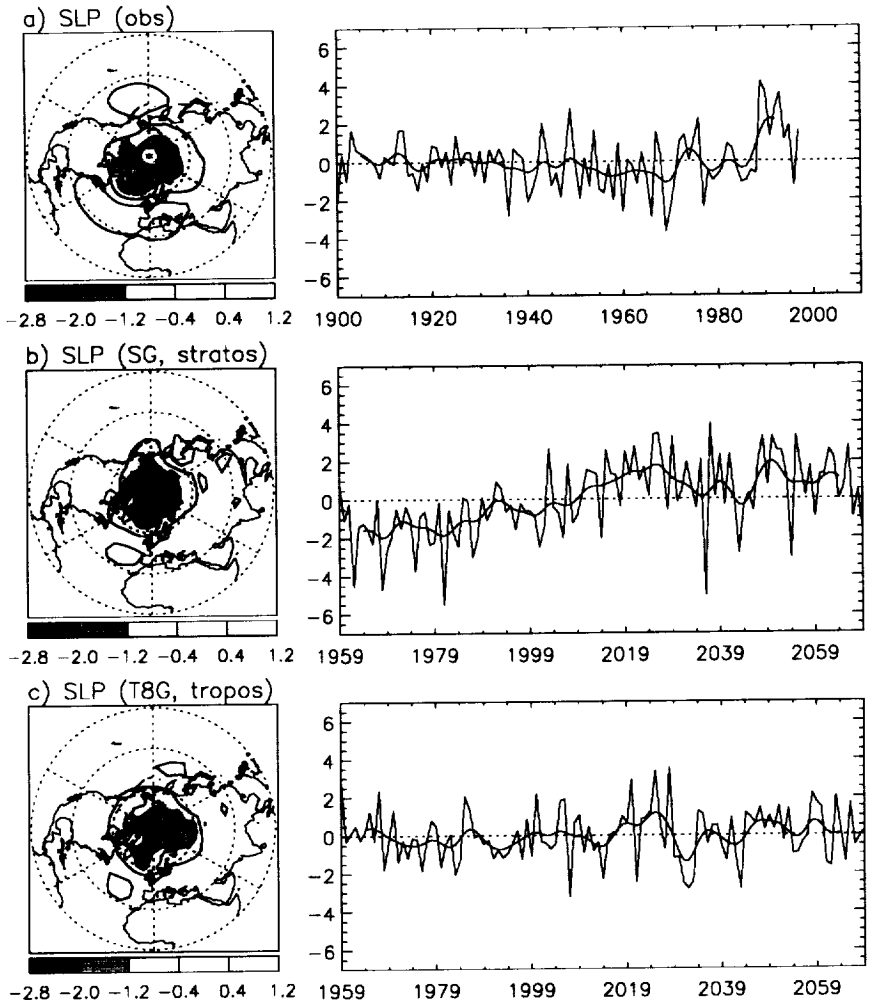

Figure 3. Northern Hemisphere sea level pressure trends. The left column shows the leading EOF (the AO), while the right column shows the principle component (PC) for: the observations (top), the stratospheric model (middle), and the 'tropospheric' model (bottom). The PCs are scaled to have units of mbar and the spatial pattern has unit amplitude poleward of 60°N. The red curve is a 10-year smoothed fit to the PC. Note that this figure is similar to Figure 2 of *Shindell et al.* [1999a], but that in that figure the PC of observed SLP was inconsistently scaled with respect to the model PCs).

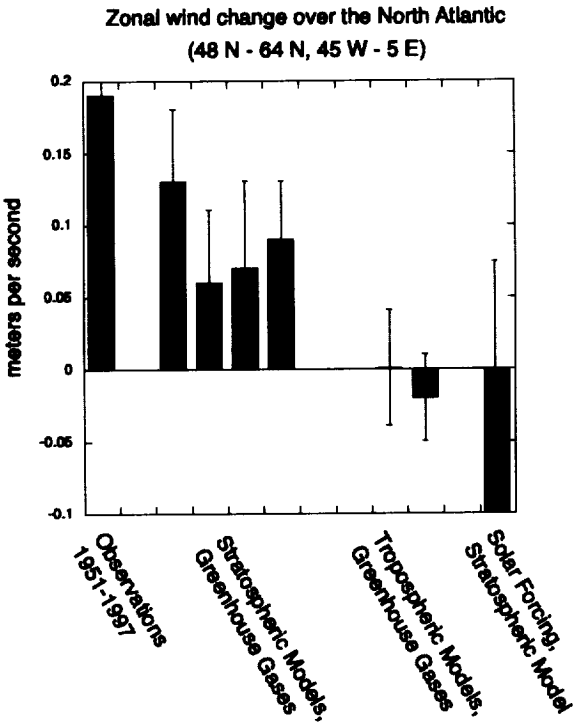

Figure 4. Observed and simulated zonal wind change over the North Atlantic (48°N – 64°N, 45°W – 5°E). Positive values are westerly winds. Values are computed as in Figure 2, except that the entire period of the NCEP reanalysis is used (1951–1997), compared with the trend over the entire length of the model simulations.

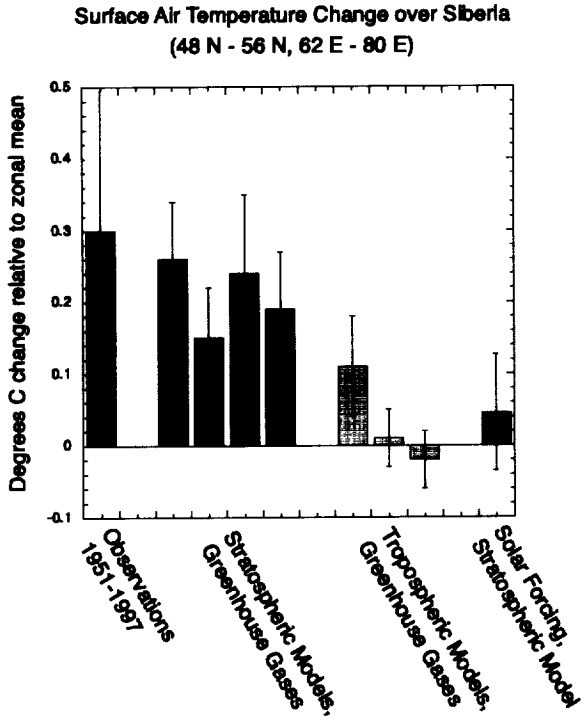

Figure 5. Observed and simulated surface air temperature change over Siberia (48°N – 56°N, 62°E – 80°E). Values are difference between the average over this location and the 48°– 56°N zonal mean in order to separate the regional signal from the latitudinal average. Values are computed as in Figure 4.

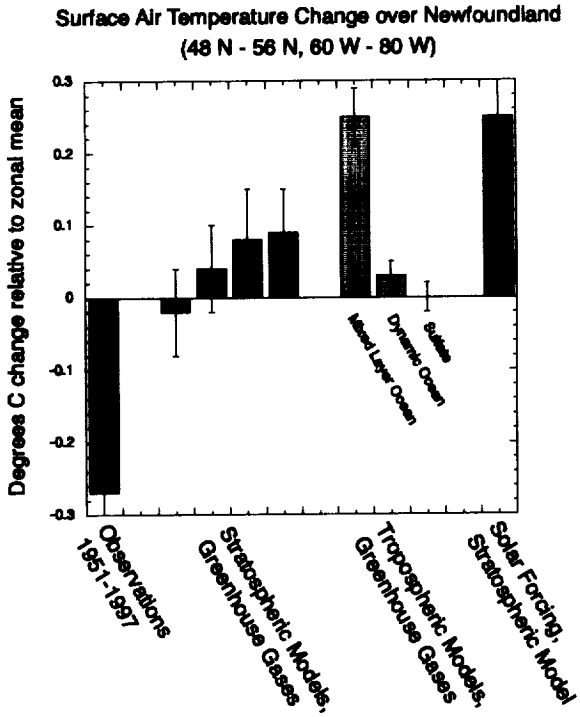

Figure 6. Observed and simulated surface air temperature change over Newfoundland (48°N – 56°N, 60°W – 80°W). As in Figure 4, values are difference between the average over this location and the 48°– 56°N zonal mean in order to separate the regional signal from the latitudinal average. Values are computed as in Figure 4.

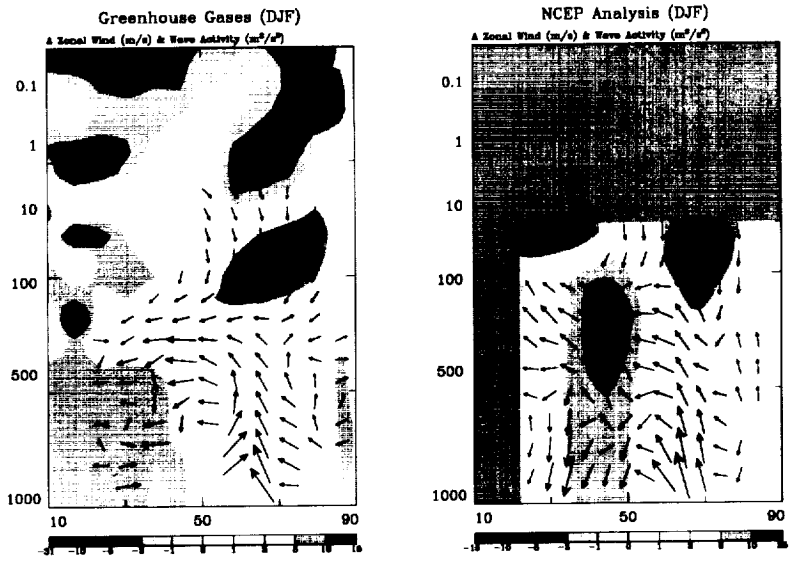

Figure 7. Trends in zonal mean zonal wind (m/s) and planetary wave activity (m^2/s^2) in the greenhouse gas simulations (left) and in analyzed observations. Model trends are shown for the five decades during which the AO increased steadily between the initial spinup and eventual saturation. Observed trends are differences between the high AO years 1981, 1983, 1984 and the low AO years 1979, 1982, and 1992 using NCEP analyses of observational data. Values are the sum of the total trend components in the first two EOFs of these trends, as given in *Ohhashi and Yamazaki* [1999], figures 7 and 8 (in a more recent paper, *Hartmann et al.* [2000] show similar results). Since the first two EOFs contain nearly all the variability, these should be comparable to the model's total trend values. Vertical fluxes have been scaled by the inverse of pressure for convenience in all plots. The maximum vector length corresponds to 7 m^2/s^2. The total AO index change in the model over this five decade period was about 4 mb, somewhat larger than the 1979 to 1992 variability of about 2.5 mb.

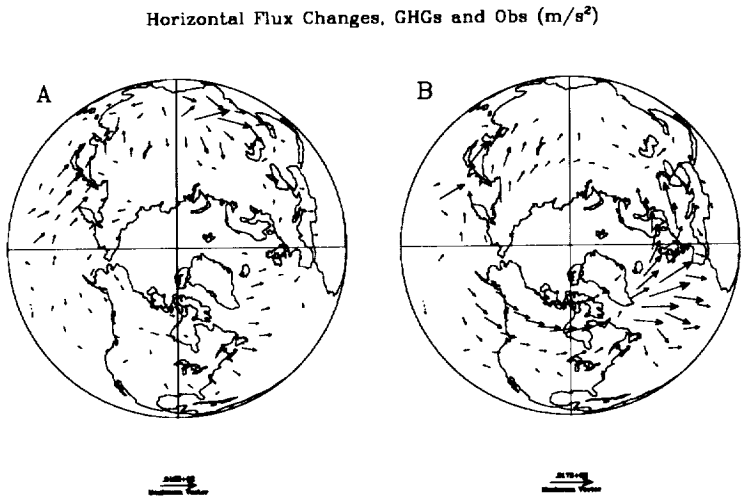

Figure 8. Horizontal wave activity flux trends (m^2/s^2) at 584 mb in the model and at 500 mb in observations. Model results are as in Figure 6. Observations are the difference between the five year means of 1989–1993 and 1965–1969, providing an estimate of the long-term trend (identical to Fig. 12b, *Kodera et al.* [1996]). The maximum vector length corresponds to 24 m^2/s^2.

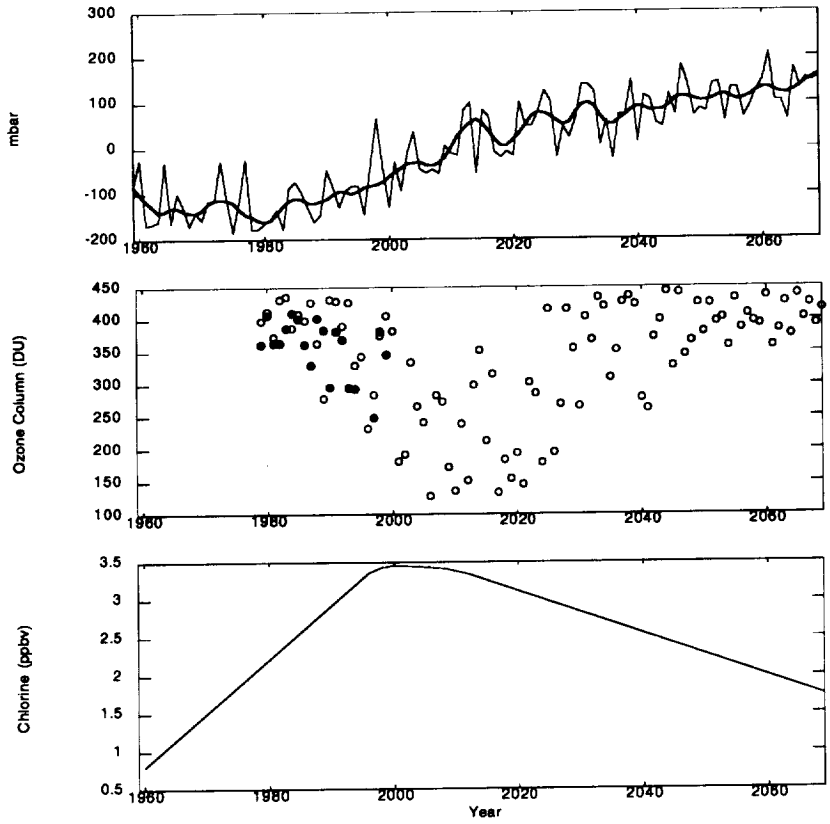

Figure 9. Trends in the strength of the Arctic vortex, Arctic ozone depletion, and stratospheric chlorine loading. The top panel shows the cold-season (November-April) averaged principle component of the leading EOF of 30 mb geopotential height from the stratospheric model with increasing greenhouse gases only, with the 10-year running mean displayed as a thicker line. The middle panel shows minimum column ozone (DU) north of 65°, averaged over the last three days of March, as seen in TOMS data through 2000 (filled circles) and in the model (open circles). Note that model values do not include intrusions of low-ozone air from lower latitudes into the Arctic, so they tend to be on the high side of observed values. The bottom panel shows the past and projected lower stratospheric chlorine loading used in the model (independent of height or latitude) based on *World Meteorological Organization* [1999]. TOMS data obtained from NASA Goddard Space Flight Center via `http://jwocky.gsfc.nasa.gov`. While ozone loss is often greatest at the end of March, in 2000, ozone column values below 250 DU were seen in early March, but did not last until the end of the month.

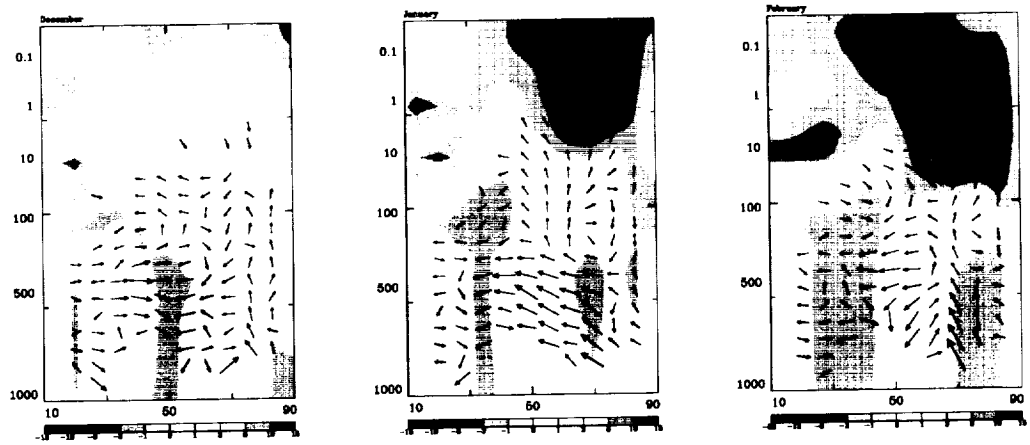

Figure 10. Differences in zonal mean zonal wind (m/s) and planetary wave activity (m^2/s^2) in the solar cycle simulations (solar maximum minus minimum). Maximum vector length corresponds to 4.2 m^2/s^2.

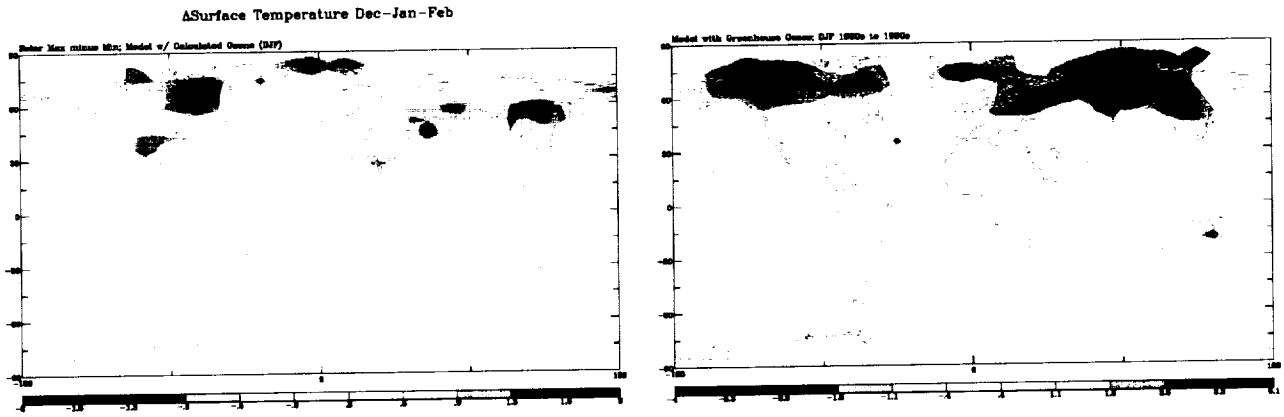

Figure 11. Latitude versus longitude December-February surface temperature changes between solar maximum and minimum (top), and from a run with increasing greenhouse gases (bottom). Small values are white. Note that the solar cycle simulations used fixed sea-surface temperatures, limiting their response.

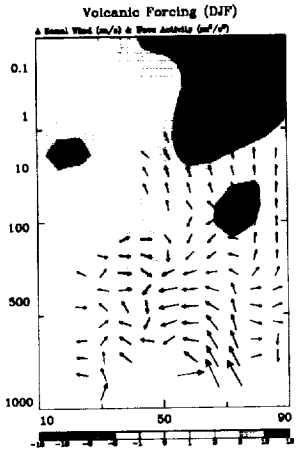

Figure 12. Differences in zonal mean zonal wind (m/s) and planetary wave activity (m^2/s^2) between volcanic and background years. Maximum vector length corresponds to 3.4 m^2/s^2.